A New Thickness Shear Mode Vibratory Gyroscope with Acoustic Gaps Between Pairs of Electrodes

Yook-Kong Yong, Mihir Patel
Dept. of Civil and Environmental Engineering
Rutgers University
Piscataway, New Jersey, U.S.A.
yyong@rci.rutgers.edu

Shigeo Kanna, Masako Tanaka, Tsutomo Imai
Seiko Epson Corporation
Suwa City, Nagano Prefecture
Japan

Abstract—**A new thickness shear mode vibratory gyroscope which employed the thickness shear mode at both the driving and sensing electrodes was presented. The thickness shear mode shape changed slightly with the Coriolis force, and this change could be detected by the sensing electrode separated from the driving electrode by an acoustic gap. Vibrating tines normal to the plate surface were placed along the acoustic gap. These tines were tuned to resonate with the harmonic Coriolis force caused by the angular rotation of the plate about its plate thickness axis. The change in vibration of the tines with the Coriolis force caused a change in charge or voltage at the sensing electrodes. Since the AT-cut resonators are known to have good f-T curves and long term aging, the new AT-cut gyroscope would have the advantages of a highly stable quartz AT-cut resonator.**

I. INTRODUCTION

In general, vibratory gyroscopes have a main driving mode and a sensing mode. When the gyroscope was given an angular velocity, the main driving mode was required to interact with the angular velocity to produce the harmonic Coriolis force that excited the sensing mode. The excitation of the sensing mode in turn produced the corresponding change in charge or voltage at the sensing electrode. The vibratory gyroscopes based on tuning forks are quite successful [1]. These gyroscopes, including those based on beams, faced some practical problems because their sensing modes were easily influenced by the mounting supports and lead installation of the sensing element. A vibratory gyroscope with a trapped energy thickness mode as the main driving mode offered good improvements in terms of frequency stability and less dependence on the mounting supports and lead installation of the sensing element.

We propose a new thickness shear mode vibratory gyroscope which uses the thickness shear mode at both the driving and sensing electrodes. The thickness shear vibrations under the sensing electrode are acoustically coupled to the thickness shear vibrations under the driving electrode via a narrow acoustic gap. The thickness shear mode shape changes slightly with the Coriolis force, and this change could be detected by the sensing electrode. This new gyroscope is based on the sensitivity of the acoustic gap to vibrations of tines located at the said acoustic gap. An AT-cut gyroscope based on these operational principles would have the advantages of a highly stable quartz AT-cut resonator with good f-T curves and good long term aging.

II. QUARTZ AT-CUT MONOLITHIC FILTERS

The arrangement of two pairs of electrodes in a two-port AT-cut monolithic filter is quite similar to that of our new AT-cut gyroscope. The two-port monolithic filter consists of two pairs of electrodes fabricated on a single quartz plate; one pair (top and bottom electrodes) is the input while the second pair is the output. The spacing of the first pair of electrodes from the second pair is the acoustic gap. If the acoustic gap is sufficiently large (usually greater than the thickness of the resonator), then each pair of electrodes can be regarded as an independent energy trapped thickness shear resonator, with little or no interaction between the two resonators [2, 3].

As the gap between the electrode pairs is reduced, the evanescent wave associated with one resonator will extend into the region occupied by the other and vice-versa. This can be explained in the terms of energy being transmitted from one resonator to the other, which results in the acoustic coupling between the resonators. Hence, one of the parameters for designing the monolithic filter is the acoustic gap.

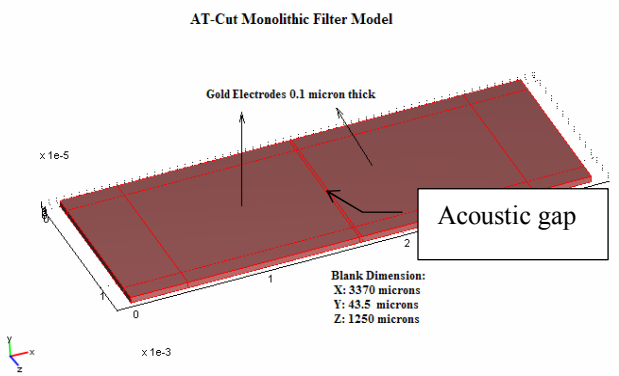

We gratefully acknowledge funding from Seiko Epson Incorporated.

Figure 1. A quartz AT-cut, two-port monolithic filiter and its dimensions.

A. *Behavior of a monolithic filter with respect to the varying width of the acoustic gap.*

The performance of a monolithic filter is dependent on the energy transition from one electrode pair to another electrode pair. This transition of energy is a direct function of the acoustic gap between the two electrodes. It is generally known that the acoustic gap should not exceed 1.15 times the plate thickness of the resonators.

Fig. 1 shows the dimensions of a 37 MHz, quartz AT-cut, monolithic filter, and the placement of the input and output electrode pairs separated by a lateral acoustic gap. Free vibration analysis was carried out with respect to the width of acoustic gap. Plots showing the effects of varying the width of acoustic gap on the resonant frequencies would be useful here. Fig. 2 has three plots showing the effects of varying the width of acoustic gap in the monolithic filter of Fig. 1: (1) the first (top) plot shows the frequencies of the resonant modes as a function of the width of acoustic gap, (2) the second (middle) plot shows the ratio of the energy under the electrodes to the total energy of resonant modes versus the width acoustic gap, and (3) the third (bottom) plot shows the ratio of energy in the acoustic gap to the total energy of resonant modes versus the width of acoustic gap. The middle plot shows the filter response in terms of energy trapping, while the bottom plot shows the filter response in terms of the relative amount of energy in the acoustic gap.

In the top plot of Fig. 2, a red modal branch is observed along with a blue modal branch at a higher frequency. The mode shape of the red modal branch is the fundamental filter mode shown in the left plot of Fig. 3. The right plot of Fig. 3 shows overtone filter mode. The vibrations of these filter modes are thickness shear vibrations. The middle plot of Fig. 2 shows that the filter modes have high energy trapping. Interestingly, the bandwidth of the filter response is given by the frequency difference between the red modal branch and the blue modal branch.

The middle and bottom plots of Fig. 2 show that not all acoustic gaps are suitable for a good filter response. There is a range of acoustic gaps from 32 to 35 microns which would yield poor filter responses. Fig. 4 shows the different frequency responses for acoustic gaps of 25 microns and 30 microns. The left plot for an acoustic gap of 30 microns shows a higher voltage gain when compared to the right plot for an acoustic gap of 25 microns.

In the next section, a new thickness shear mode vibratory gyroscope is proposed using the two pairs of electrodes like those in the two-port monolithic filter.

III. A New Thickness Shear Mode Vibratory Gyroscope with Acoustic Gaps Between Pairs of Electrodes

Fig. 5 shows a 5 MHz quartz AT-cut thickness shear mode vibratory gyroscope with two pairs of electrodes separated laterally by an acoustic gap. The gyroscope employs the input electrode and output electrode of the two-port monolithic filter as the driving electrode and sensing electrode, respectively.

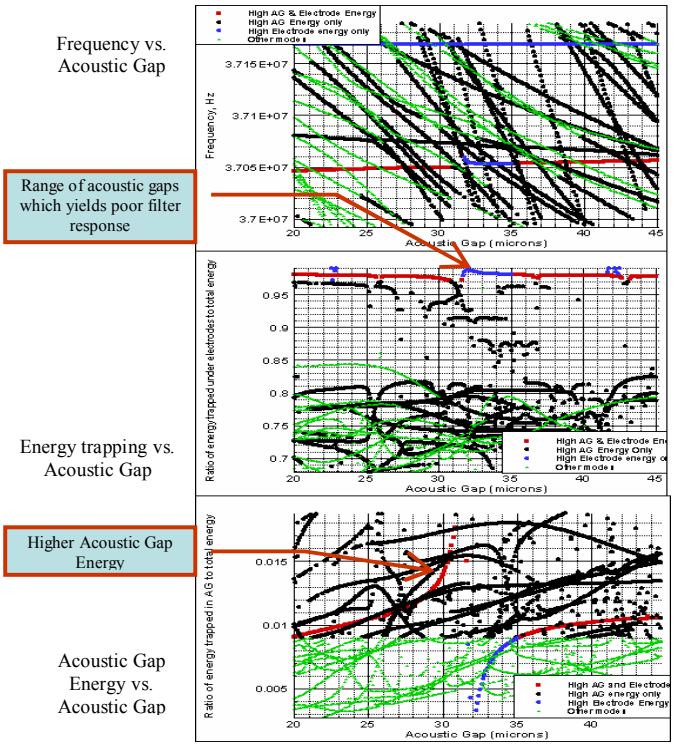

Figure 2. Frequency of resonant modes, energy trapping ratio, and acoustic gap energy versus the acoustic gap width for the two-port filter of Fig. 1.

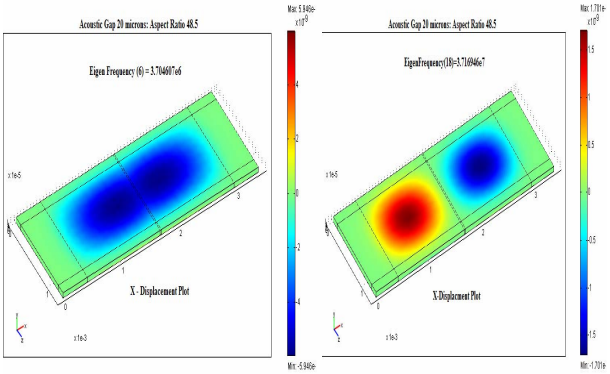

Figure 3. Mode shapes of the fundamental filter mode (left), and its first overtone filter mode (right) of the two-port monolithic filter of Fig. 1.

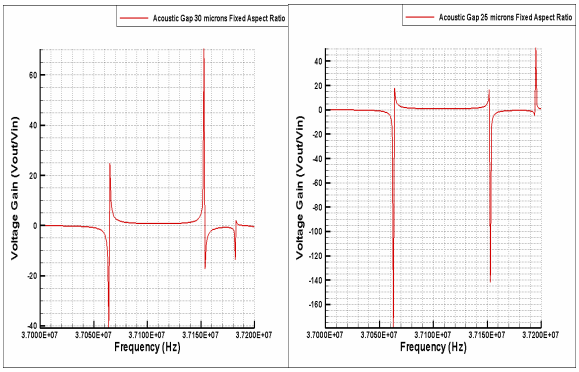

Figure 4. Frequency responses for two acoustic gap widths.

A row of tines are embedded along the acoustic gap. These tines could be designed to vibrate at the driving frequency and respond to the angular velocity of the gyroscope about its plate thickness axis.

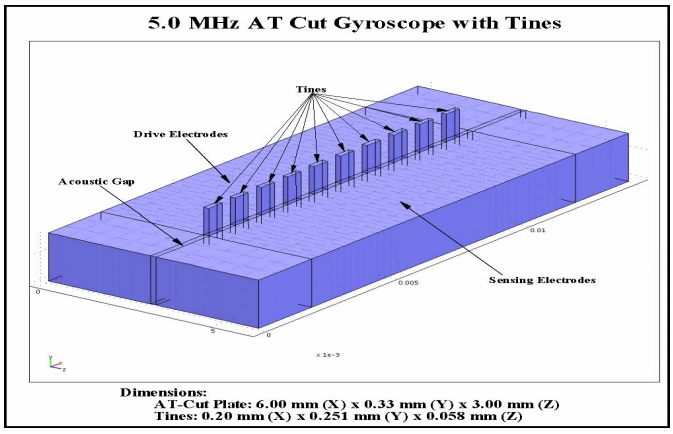

Figure 5. A 5 MHz quartz AT-cut thickness shear gyroscope with a row of tines along the acoustic gap between the driving and sensing electrodes.

A. *Governing Equations for the Quartz AT-cut Thickness Shear gyroscope*

The three-dimensional governing equations for piezoelectricity for quartz with mechanical damping and resistance in current conduction by Lee, Liu and Ballato [4] are employed in the modeling of the AT-cut gyroscope.

1) Strain-Displacement Equationss:

$$E_{ij} = \frac{1}{2}\left(u_{i,j} + u_{j,i}\right) \tag{1}$$

2) Stress-Strain Constitutive Equaitons:

$$T_{ij} = C_{ijkl}\, E_{kl} + e_{pij}\, \phi_{,p} + \eta_{ijkl}\, \dot{E}_{kl} \tag{2}$$

3) Electrostatic Constitutive Equations:

$$D_i = e_{iq}\, E_q - \varepsilon_{ik}\, \phi_{,k} \tag{3}$$

$$J_i = -\sigma_{ik}\, \phi_{,k} \tag{4}$$

4) Stress Equations of Motion:

$$T_{ij,j} = \rho \ddot{U}_i \tag{5}$$

5) Charge Equations:

$$\dot{D}_{i,i} + J_{i,i} = 0 \tag{6}$$

In these equations, E_{ij} is the strain, T_{ij} is the stress, u_i is the mechanical displacement, D_i is the electric flux density and ϕ is the electric potential. C_{ijkl} are the elastic stiffness constants at constant electric field, e_{pij} are the piezoelectric stress constants, ε_{ik} are the dielectric permittivities, and ρ is the mass density. Also, in these equations, J_i is the current density, η_{ijkl} are the viscosity coefficients, σ_{ik} are the electric conductivities, and $\dot{E}_{kl}$ is the strain rate. The materials values of the viscosity coefficients η_{ijkl} were measured by Lamb and Richter [5], while those of the electric conductivities σ_{ik} for the AT-cut quartz were estimated by Lee, Liu, and Ballato [4].

The analysis of gyroscopes using finite elements is well established; the paper by Kagawa, Tsuchiya, and Kawashima [6] provides a good reference. The weak form of the above set of equations was formulated and implemented in the finite element software COMSOL Multiphysics.

B. *Gyroscope in Angular Velocity – Coriolis Force*

When the gyroscope vibrates at a constant frequency ω, all its material points vibrate with displacements $\underline{u}(\underline{x})e^{j\omega t}$ where $\underline{u} = (u_x, u_y, u_z)$, are the displacement magnitudes at the spatial location $\underline{x} = (x, y, z) = (x_1, x_2, x_3)$. When the gyroscope is rotated about its plate thickness axis (y-axis) with an angular velocity Ω, a Coriolis body force is generated at all the material points with velocities $j\omega \underline{u}(\underline{x})e^{j\omega t}$:

$$\begin{aligned} b_x &= 2\Omega\rho\,(j\omega u_z e^{j\omega t}) \\ b_y &= 0 \\ b_z &= -2\Omega\rho\,(j\omega u_x e^{j\omega t}) \end{aligned} \tag{7}$$

We note that the Coriolis body forces in (7) are also harmonic at the frequency ω which is also the driving frequency of the gyroscope. Here in (7) the centrifugal force was neglected since $\omega >> \Omega$.

IV. Vibrations of the Tines along the Acoustic Gap

The tines are prismatic bars normal to the plate surface and embedded along the acoustic gap. They are essential for detecting the angular rotation of the gyroscope about its plate thickness axis. They must be designed to resonate at the driving frequency ω which is the frequency of the fundamental filter mode. When the gyroscope is angularly rotated about its y-axis, and the tines vibrate in the z direction, then a body Coriolis force b_x given by the first equation of (7) is generated in the tines. The tines, in order to sense this angular velocity Ω, must have a sensing mode with a mode shape similar to the Coriolis force b_x, and a frequency as close as possible to the driving frequency. Similarly, if the tines

vibrate in the x direction, a body Coriolis force b_z given by the third equation of (7) is generated in the tines; and the tines, in order to sense the angular velocity Ω, must have a sensing mode with a mode shape similar to the Coriolis force b_z, and a frequency as close as possible to the driving frequency.

Fig. 6 shows the fundamental filter mode (driving) mode of the gyroscope of Fig. 5 at the driving frequency of 4.857 MHz. The tines vibrate predominantly in the z-direction; however there is also an x-direction displacement component as shown by the color contours. Fig. 7 shows the sensing mode at 4.856 MHz where the tines also vibrate predominantly in the z-direction with an x-direction displacement component shown by the contour colors. The difference between the driving and sensing modal frequencies is about 1 KHz. *This configuration of the tines and plate resonator represents a novel vibratory gyroscope.*

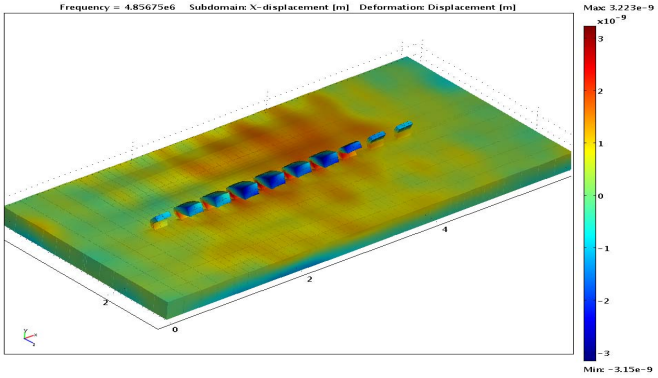

Figure 6. Mode shape of the gyroscope at the driving frequency of 4.857 MHz. Tines have large displacement magnitudes in the x- and z-directions.

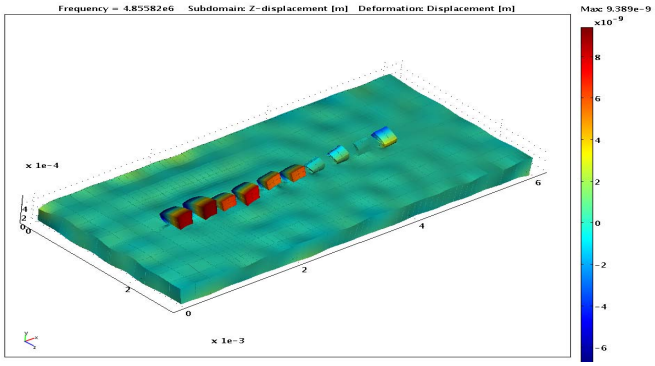

Figure 7. Mode shape of the gyroscope at the sensing frequency of 4.856 MHz. Tines have large displacement magnitudes in the x- and z-directions.

A. Free Vibration Analysis of the Gyroscope for Various Geometries of the Tines

Free vibration analysis was performed on the 5.0 MHz gyroscope with tines (Fig. 5) using the tines dimensions as parameters. The analysis is needed for determining tines dimensions which yield suitable resonant modes with frequencies close to the thickness shear mode frequency. In the next three figures, the effects of the width, length and height dimensions of the tines are investigated.

Fig. 8 shows the frequencies of resonant modes in the vicinity of the fundamental and first overtone filter modes (red) for width of acoustic gap varying from 0.1 mm to 0.5 mm. This figure shows that the acoustic gap widths greater than 0.34 mm are not useful for the gyroscope because the fundamental filter mode is poorly defined, and not well energy trapped. The figure is also useful for determining the tines modes (green) which have resonant frequencies close to the frequency of the fundamental filter mode: these occur at locations where the modal branches for the tines cross the modal branch of the fundamental filter mode.

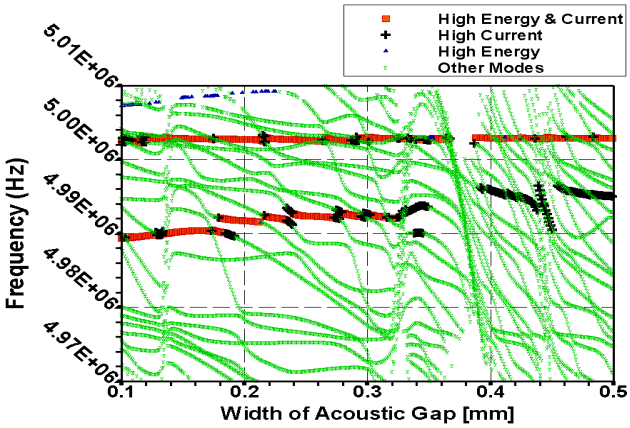

Figure 8. Frequencies of resonant modes versus the width of acoustic gap. The length (x-dimension) and height (y-dimension) of the tines are fixed at 0.2 mm, and 0.337 mm, respectively.

Fig. 9 shows the frequencies of resonant modes in the vicinity of the fundamental and first overtone filter modes (red) for length (x-dimension) of tines varying from 0.15 mm to 0.4 mm. This figure shows that for tines length of 0.32 mm to 0.33 mm the fundamental filter mode is not well defined due to the strong modal interactions. The figure is also useful for determining the tines modes (green) which have resonant frequencies close to the fundamental filter mode frequency.

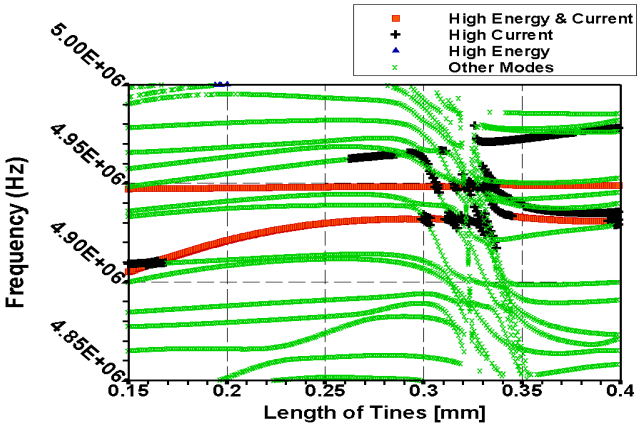

Figure 9. Frequencies of resonant modes versus the length (x-dimension) of the tines. The acoustic gap width (z-dimension) and height (y-dimension) of the tines are fixed at 0.09 mm, and 0.337 mm, respectively.

Fig. 10 shows the resonant modes in the vicinity of the fundamental filter mode (red) for height (y-dimension) of tines varying from 0.24 mm to 0.26 mm. The figure is useful for

determining the suitable tines modes (green) which have resonant frequencies close to the frequency of the fundamental filter mode.

By employing the plots like those from Figs. 8, 9 and 10 we can find the dimensions of tines which would yield strong sensing responses at the driving frequency of the gyroscope.

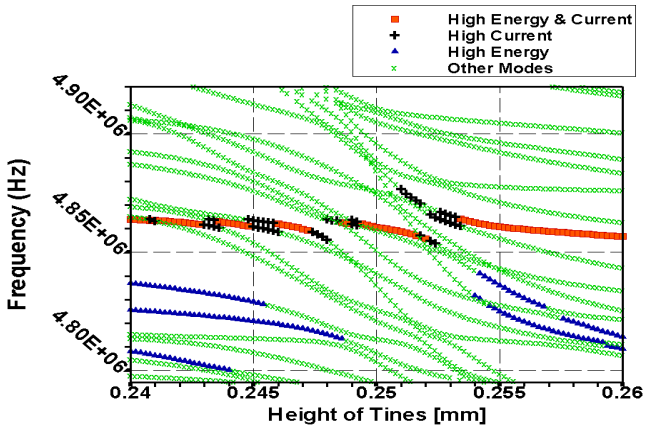

Figure 10. Frequencies of resonant modes versus the height (*y*-dimension) of the tines. The acoustic gap width (*z*-dimension) and length (*x*-dimension) of the tines are fixed at 0.058 mm, and 0.2 mm, respectively.

V. Frequency Response Analysis of the Quartz AT-cut Gyroscope with Tines

A forced vibration analysis, or frequency response analysis, of the gyroscope is required in order to study the feasibility of the new gyroscope. The analysis was carried out in two steps: (a) the forced vibration of the gyroscope without angular velocity (no Coriolis force), and (b) forced vibration of the gyroscope with angular velocity (with Coriolis force). The difference in charge or voltage at the sensing electrode between step (a) and step (b) gives the response of the gyroscope to the angular velocity.

The frequency responses of three different heights of the tines were investigated for the short circuit and open circuit conditions at the sensing electrode. For the short circuit condition, the charge at the sensing electrode was calculated; while for the open circuit condition, the voltage at the sensing electrode was calculated. The table below shows the three sets of tines dimensions.

TABLE I. Three Sets of Tines Dimensions

Set	Dimensions of the tines		
	acoustic gap, mm *z-dimension*	*Length, mm* *x-dimension*	*Height, mm* *y-dimension*
A	0.058	0.2	0.2516
B	0.058	0.2	0.2518
C	0.058	0.2	0.252

Fig. 11 shows the gyroscope frequency responses without Coriolis force in terms of the charge at sensing electrode versus the excitation frequency. The driving and sensing mode responses for each tine height are noted on the plot. We observe that for the tine height of 0.2518 mm the driving and sensing mode frequencies are the closest to each other. When an angular velocity of 60 deg./s was applied, there were small changes in the charge at sensing electrode. Fig. 12 shows the change in magnitude of the charge at sensing electrode, and we observe that for the tine height of 0.2518 mm the change in magnitude of charge is the greatest.

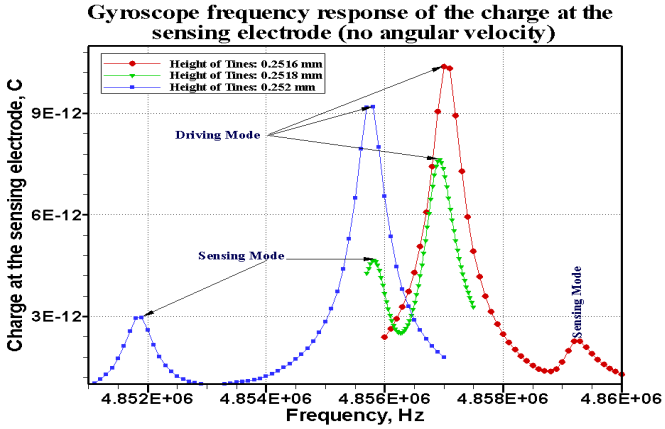

Figure 11. Gyroscope frequency response of the charge at the sensing electrode (no angular velocity).

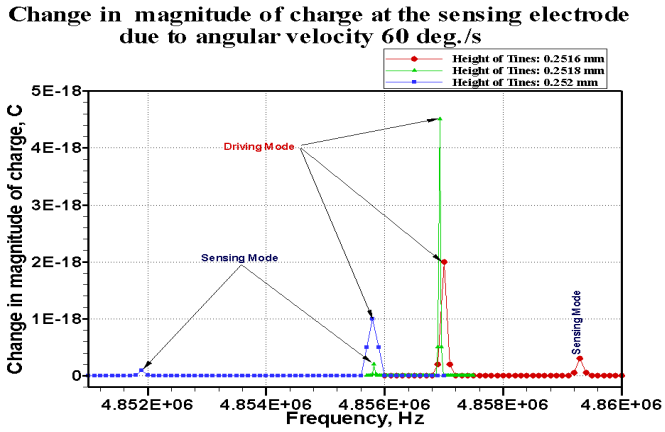

Figure 12. Change in magnitude of charge at the sensing electrode due to an angular velocity of 60 deg./s

Fig. 13 shows the gyroscope frequency responses without Coriolis force in terms of voltage at the sensing electrode versus the excitation frequency. We observe that for the tine height of 0.2516 mm the driving and sensing mode frequencies are the closest to each other. When an angular velocity of 60 deg./s was applied, there were small changes in the voltage at the sensing electrode. Fig. 14 shows the change in magnitude of voltage at the sensing electrode, and we observe that for the tine height of 0.2516 mm the change in magnitude of voltage is the greatest.

Figs. 12 and 14 show that the closer the frequency of tines sensing mode is to the frequency of gyroscope driving mode, the stronger the gyroscope responds to an angular velocity.

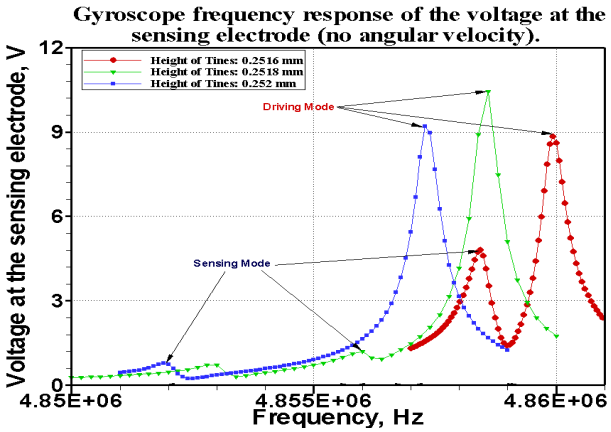

Figure 13. Gyroscope frequency response of the voltage at the sensing electrode (no angular velocity).

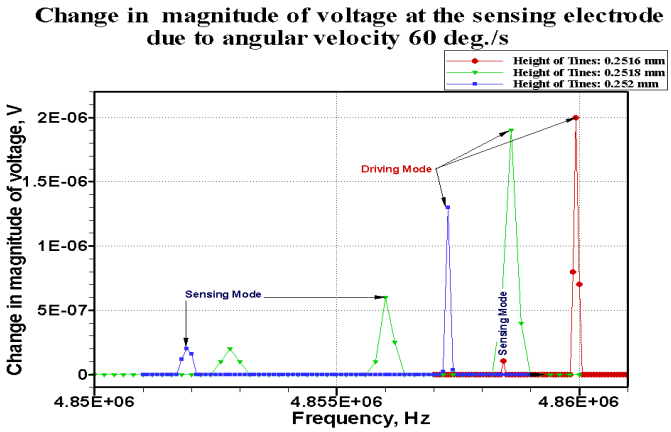

Figure 14. Change in magnitude of voltage at the sensing electrode due to an angular velocity of 60 deg./s

VI. Sensitivity of the Gyroscope

A useful parameter for determining the feasibility of a gyroscope is its sensitivity to the angular velocity. We could also determine whether the sensitivity curve is linear. The sensitivity in change of charge and voltage was investigated with respect to the angular velocity. Fig. 15 shows the sensitivity in change of charge of the gyroscope Set B with respect to angular velocity, and a sensitivity of 8.33×10^{-20} C/deg./s was obtained. Fig. 16 shows the sensitivity in change of voltage of the gyroscope Set B with respect to angular velocity, and a sensitivity of 3.33×10^{-8} V/deg./s was obtained.

VII. Summary and Conclusion

A new thickness shear mode vibratory gyroscope which employed the thickness shear mode at both the driving and sensing electrodes was presented. The driving and sensing electrodes operate in a similar principle to the input and output electrodes, respectively, of a two-port monolithic filter. The thickness shear mode shape changed slightly with the Coriolis force produced by vibrating tines placed along the acoustic gap. Free vibration analysis was performed to determine the suitable dimensions of tines. Forced vibration analysis was performed to determine the gyroscope response and its sensitivity. The 5 MHz AT-cut gyroscope was found to respond to the angular velocity, however the sensitivity was found to be small. Better sensing and driving modes of the tines are needed to increase the gyroscope response.

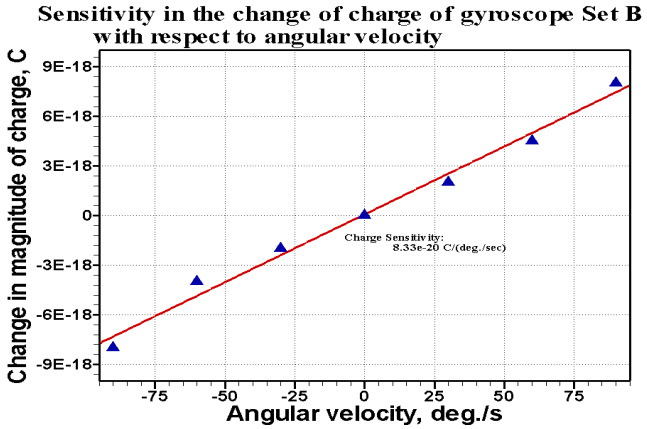

Figure 15. Sensitivity in the change of charge of gyroscope Set B with respect to angular velocity.

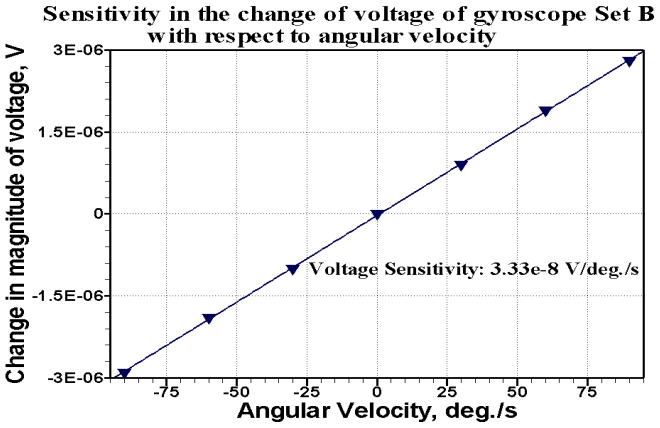

Figure 16. Sensitivity in the change of voltage of gyroscope Set B with respect to angular velocity.

References

[1] K. Sato, A. Ono, and Y. Tomikawa, "Experimental study of gyro sensor using double0ended tuning fork quartz resonator," Japanese Journal of Applied Physics, Vol. 43, No. 5B, 2004, pp. 3000-3003.

[2] R.A.Sykes and W.D.Beaver,"High freqeuncy monolithic crystal filters with possible application to single frequency and single side band use", Proc. 20th Ann. Symp. Frequency Control, 1966, pp. 288-308.

[3] W.D.Beaver,"Analysis of elastically coupled piezoelectric resonator",Journal of the .Acoustical Society of America,Vol. 43, May 1968, pp. 972-981.

[4] P.C.Y. Lee, N.H. Liu and A. Ballato, "Thickness vibrations of piezoelectric plates with dissipation", IEEE Transactions on Ultrasonics, Ferroelectrics and Frequency Control, Vol.51, January 2004, pp. 52-62.

[5] J. Lamb and J. Richter, "Anisotropic acoustic attenuation with new measurement for quartz at room temperatures", Proceedings of the Royal Society, 293A, pp. 479-492, 1966.

[6] Y. Kagawa, T. Tsuchiya, and T. Sakai, "Three-dimensional finite element simulation of a piezoelectric vibrator under gyration," IEEE Transactions on Ultrasonics, Ferroelectrics, and Frequency Control, Vol. 48, No. 1, January 2001, pp. 180-188.